Effects of microalgae -ethanol-methanol-diesel blends on the spray characteristics and emissions of a diesel engine

Upendra Rajak[1] · **Abhishek Dasore**[1] · **Prem Kumar Chaurasiya**[2] ·
Tikendra Nath Verma[3] · **Prerana Nashine**[4] · **Anil Kumar**[5]

Abstract

In the current investigation, fuel blend combination (FBC) of *spirulina microalgae* bio-diesel (SMAB), diesel, ethanol, and methanol is prepared and assessed. Engine performance and spray attributes of FBC were investigated through Diesel-RK Software (DRS) at different engine loads using FBC0, FBC1, FBC2, FBC3, FBC4, FBC5, and FBC6. The viscosity of SMAB decreased with the addition of alcohol. Increasing percentage of SMAB from 0 to 40% in the FBC increases the spray characteristics by 11.9%. Performance of engine was enhanced by adding ethanol and menthol to SMAB and diesel combinations. Brake thermal efficiency (BTE) and brake specific fuel consumption (BSFC) were 1.7% higher and 6.6% lower for FBC6 blend compared to FBC0 (diesel fuel). Increase in percentage of SMAB, ethanol, and methanol in hybrid fuels has shown a decrease in smoke emissions, NO_X emissions by 41.3 and 43% at various engine loads.

Nomenclature

BTE   Brake thermal efficiency
BSFC   Brake specific fuel consumption
CO   Carbon monoxide
DRS   Diesel-RK Software

✉ Prem Kumar Chaurasiya
   prem.chaurasiyaa@gmail.com

✉ Tikendra Nath Verma
   verma.tikks@gmail.com

1   School of Mechanical Engineering, RGM College of Engineering and Technology, Nandyal 518501, India

2   Department of Mechanical Engineering, Bansal Institute of Science and Technology Anand Nagar Bhopal, Bhopal, M.P, India

3   Department of Mechanical Engineering, Maulana Azad National Institute of Technology, Bhopal 462003, India

4   Department of Mechanical Engineering, National Institute of Technology, Rourkela 769008, India

5   Department of Mechanical Engineering, Delhi Technological University, Delhi 110042, India

DOD	Diameter of drops
FBC	Fuel blend combination
FBC0	100% diesel fuel
FBC1	80% diesel fuel and 20% *spirulina microalgae* biodiesel
FBC2	FBC2
FBC3	60% diesel fuel and 40% *spirulina microalgae* biodiesel
FBC4	80% FBC1 and 20% ethanol
FBC5	80% FBC1 and 20% methanol
FBC6	80% FBC2 and 20% methanol
FSTP	Free spray tip penetration
HSL	Hartridge smoke level
IC	Internal combustion
PCP	Peak cylinder pressure
SCA	Spray cone angle
SOE	Summary of emission
SMAB	Spirulina microalgae biodiesel
X_i	Mixing ratio of fuel
ρ_b	Density of blend
ρ_i	Known density of fuel component
σ	Surface tension
CN_b	Cetane number of blend
CI_i	Known cetane number of fuel component
HV_b	Lower heating value of blend
HV_i	Known lower heating value of fuel component
η_b	Kinetic viscosity of blend
η_i	Known kinetic viscosity of fuel component
VBI_b	Viscosity blend index

1 Introduction

Alternative fuels are getting attention as optimistic supportable energy foundations to replacing fossil fuels due to the strict restrictions through legislation to reduce greenhouse gas emissions while preserving the natural resources (Rajak et al., 2019). The usage of petroleum-based fuels is rising every day. Researches have already reported that 84% of carbon emissions have been released to the atmosphere since 1980s from petroleum-based fuels (Celebi et al., 2019). The utilization of compression ignition engines in the automobile sector is still widespread. One technique to enhance the percentage use of alternative fuels is to employ 1st, 2nd, and 3rd generations alternative fuels in the automobile sector (Kuszewski et al., 2019). In this respect, many researchers have used alternative fuels belonging to the 1st, 2nd, and 3rd generations of alternative fuels (Rajak et al., 2019). Methanol and ethanol are two types of light alcohol. Ethanol is considered to be essential fuel for IC engines due to more content of oxygen.

The effects of biodiesel-diesel-ethanol (BDE) mixes fuel with various oxygenates and viscosity-lowering additives, such as ethanol, with diesel or biodiesel fuel by ethanol concentration (5 to 10%), on diesel engine performance and emissions have been investigated (Krishna et al., 2019). On a single-cylinder light-duty (LD) CI engine, the effects of oxygenates with diesel, biodiesel, and EtOH in the ratios of 68:17:15 and 58:14:30 were

investigated. When using the fuel with the highest content of EtOH, the result showed a significant reduction in soot-NOX emissions (Shamun et al., 2018). The effects of ethanol on diesel engine performance indicators were investigated, and it was discovered that ethanol-blended diesel fuel reduced engine brake power (Khoobbakht et al., 2019). Examined the fragmentation and nozzle flow features of fuel blends of biodiesel-ethanol. They found a reduction in ignition delay period and peak injection rate due to fuel properties. The results improved in atomization performance of ethanol addition with biodiesel fuel (Park et al., 2010). Used blends of alcohols, biodiesel, and diesel and evaluated engine properties with fluctuating loads. The outcome of their work shows that the exhaust gas emission was diminished with all tested fuel. The engine performance is enhanced with fuel blends of methanol and diesel (Ghadikolaei et al., 2018). Assessed the effects of ethanol-blended biodiesel fuel using CI engine under various engine speeds (1250-3500 rpm). They obtained reduced engine brake power and torque fuelled with 5% biodiesel and 20% ethanol mixture (B5E20) fuel (Kandasamy et al., 2019). Analysed oleaginous microalga (Chlorella vulgaris) for biomass, lipid production, and fatty acid in both mixotrophic and photoautotrophic settings. The microalgal biomass was grown mixotrophically and photoautotrophically. In photoautotrophic culture, atmospheric CO2 was the sole source of carbon and energy, while molasses was employed in mixotrophic cultivation. The microalgal biomass was extracted after 5 days of nitrogen deprivation. Mixotrophic farming produced much more biomass (137.43 13.3 mg L^{-1} day) than photoautotrophic cultivation (91.57 7.9 mg L^{-1} day). Dry mixotrophic biomass provided around 39% (w/w) of total lipid content. The extracted oil has greater polyunsaturated fatty acid contents (palmitic and oleic acids). Polyunsaturated fatty acids (60 mg g^{-1} dried algal biomass) provided high-quality biofuel production (Natasha Laraib et al., 2021). Investigation was performed to improve the acid hydrolysis of pomegranate peel waste (PPW) for ethanol production utilising CCD and RSM. The dependent variables were sulfuric acid concentration, temperature, and hydrolysis duration, whereas the responses were reducing sugars, total carbohydrates, extractives, weight loss, hemicellulose, cellulose, and lignin contents. The maximum glucose level was 0.56 mg mL^{-1} (5% acid at 100 ºC for 30 min) and carbohydrate content was 1.53 mg mL^{-1} (Ayesha Saleem et al., 2020). Examined the biomass productivity, lipid content, and fatty acid profile of an oleaginous microalga (Scenedesmus dimorphus) grown under mixotrophic conditions with apple-pomace hydrolysate as a carbon and energy source. Mixotrophic farming produced more biomass (140.37 mg L1 d1) than photoautotrophic cultivation (96.55 mg L-1 d-1). The lipid content (w/w) of mixotrophic biomass was 41% greater than photoautotrophic biomass (28%). Polyunsaturated fatty acids were more abundant in lipidome (palmitic and oleic acids). Findings will help to improve the biofuel balance by using oleaginous microalgal biomass grown in mixotrophic settings (Natasha Laraib et al., 2021).

Investigated the CI engine properties charged with diesel-ethanol and biodiesel-ethanol blends. They found higher indicated thermal efficiency for 35% ethanol fraction with diesel and biodiesel. The ignition delay was almost similar for both fuels (diesel and biodiesel). However, NO_X and unburnt hydrocarbon emissions were obtained higher for ethanol fraction on the tested engine. Reported that the increasing ethanol fraction in the fuel increases CO emissions while simultaneously reducing NO_X emissions (An et al., 2015). While the maximum engine pressure and indicated thermal efficiency was reduced because of extended ignition delay time and lesser heating value (Tutak et al., 2017). Reported that the unburnt hydrocarbon, smoke, and NO_X emissions were diminished with the aid of SMAB blends (Rajak et al., 2019). Investigated the combined effects of using ternary blend (15% ethanol-5% biodiesel-80% diesel fuel) at different speeds of the engine

(1400-2200 rpm). The outcomes indicated lessening in emissions and improvement in the engine performance (Ghadikolaei et al., 2019). Examined the impacts of hythane gas and water in a dual-fuel WiDE (Radha Krishna Gopidesi et al., 2021). The Wide reduces NOX emissions dramatically by vaporising water particles in the combustion chamber at lower temperatures. Combining methane and hydrogen (hythane) gas samples as secondary fuel has encouraging results in reducing exhaust emissions without reducing engine thermal efficiency (Radha Krishna Gopidesi et al., 2021). The performance, combustion, and emission characteristics of a 5.95 kW four-stroke direct injection diesel engine running on diesel, rapeseed oil biodiesel, and diesel–biodiesel blends were studied. The engine's performance measures such as in-cylinder pressure, heat release, and ignition delay were studied. All test fuels had unburned hydrocarbons, CO, NOx, and smoke emissions. The testing outcomes using biodiesel blends were compared to baseline diesel. The test findings showed that B25 blend may be employed in diesel engines with acceptable thermal efficiency and improved emissions (L. Anantha Raman et al., 2019). Focused on producing biodiesel from subcutaneous and intramuscular cattle tallow wastes from leather tanneries and slaughterhouses. The maximal fat content was 92.5% for subcutaneous wastes and 3.05% for intramuscular wastes, respectively. The rendered waste tallow was transformed into biodiesel utilising ethanol as a solvent and [L-Vaemim] Br as an ionic liquid catalyst. The best-optimised reaction parameters are: 1:7.5 molar ratio, 20% tallow catalyst concentration, 75 °C reaction temperature, and 160 min reaction duration (J. Ranjitha et al., 2019).

Examined combustion and electrospray properties of ethanol-biodiesel on the mesoscale combustor. The spray angle is increased and fuel droplet size was reduced with the use of ethanol. They obtained 40% of optimum ethanol blend. This study showed a reduction in CO emission due to the reduction of the droplet size, and a higher percentage of ethanol had shown better atomization (Jiang et al., 2019). Investigated characteristics in a 2-stroke engine using exhaust gas recirculation (EGR) technology at variable fuel injection time. The results showed the lower NO_X emission and provided an optimum method of workable technological for diesel engine emissions (Sun et al., 2017). Reviewed the effects of diesel-ethanol-biodiesel various operating conditions on the different characteristics of combustion, performance, emission of diesel engines (Hoseini et al., 2017). Best method for reduction of diesel engine exhaust gas emissions is using alternative fuels (biodiesel, ethanol, and diesel), but no mythology is available to reduce all the pollutants of the diesel engine (Jiao et al., 2019).

Previous investigation using SMAB, ethanol, and diesel fuel blended fuel significantly less. In the current study, the performance of the engine and spray characteristics were investigated by Diesel-RK Software (DRS). Performance and emissions characteristics of blended fuels were investigated. SMAB, ethanol, and diesel are used for fuel blended fuel. Engine spray characteristics were analysed through DRS. Engine performance is evaluated through thermal efficiency, cylinder pressure, volumetric efficiency and fuel consumption. NO_X, Hatridge smoke level and summary of emissions compared exhaust gas emissions.

2 Material and experimental protocol for validation of DRS

2.1 Material and properties

In the current work, diesel fuel, SMAB, methanol, and ethanol were employed in the CI engine as fuels. First, SMAB was blended with base fuel viz., diesel with

Table 1 Properties of fuel (Qi DH et al., 2019; Rajak U et al., 2019)

Eqs.	Name of equation	Equation
1	Measure density	$\rho_b = \sum_{i=1}^{3} X_i \rho_i$
2	Measure viscosity	$\ln v_b = \sum_{i=1}^{3} X_i \ln v_i$
3	Measure cetane number	$CN_b = \sum_{i=1}^{3} X_i CN_i$
4	Measure heating value	$HV_b = \frac{\sum_{i=1}^{3} X_i \rho_i HV_i}{\sum_{i=1}^{3} X_i \rho_i}$
5	Measure kinematic viscosity	$\eta_b = e^{\left[e^{\left(VBI_b - 10.975 \right)/14.534} \right]} - 0.8$
6	Measure surface tension	$\sigma = (49.6\rho - 14.92) \times 10^{-3}$
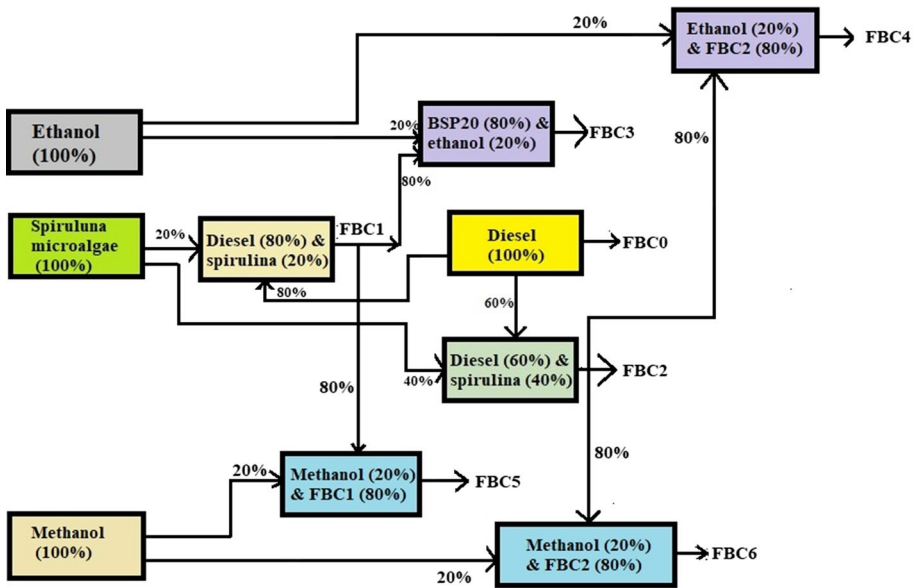
Fig. 1 Blending procedure in present study

two-volume proportions of 20% and 40% which were denoted as FBC1 and FBC2. Later, both FBC1 and FBC2 are blended with a 20% volume fraction of ethanol and methanol. The obtained blends were represented as FBC3, FBC4, FBC5, and FBC6, respectively. Blending equations are described in previous literature (Qi et al., 2019; Rajak et al., 2019) and produced the same here as shown in Fig. 1 and fuel properties are given in Tables 1 and 2.

Table 2 Fuel characteristics (Balasubramanian and Subramanian, 2019; Qi et al., 2019; Rajak et al., 2019)

Property	Diesel	SMAB	Ethanol	Methanol
CN	48-52	52.2	6-8	5.0
ρ(g/mL)	0.830	0.860	0.79-0.80	0.790
v at 40 °C (mm^2/s)	3.0	5.66	1.1	0.59
LHV (MJ/kg)	42.5	41.36	26.79-27.8	19.6
σ(N/m)	0.028	0.0277	0.0247	0.0242

2.2 Experimental setup

Tests were performed on a single-cylinder CI engine. The authentication of DRK tool is done against pressure and heat dissipation rate with non-variant speed and injection timing using diesel fuel (Rajak et al., 2020). The technical conditions of the diverse devices utilised throughout the experiments and the maximum uncertainties are shown in Tables 3 and 4. The error deviation was obtained from the equipment to aid the standard deviation equation from the study (Datta A et al., 2017). The percentage uncertainty in the measurement of various parameters is listed in Table 4 using the standard deviation equation and obtained to be ± 2.58%.

Table 5 shows the uncertainty analysis of the instrument used in the experiment. All the instruments were calibrated and uncertainty analysis was performed using uncertainty equation. Figure 2 shows the complete assembled engine used for experiment.

Table 3 Fuel blend combination (FBC) characteristics

Fuel	FBC0	FBC1	FBC2	FBC3	FBC4	FBC5	FBC6
CN	48-52	48.85	49.72	40.02	40.72	39.82	40.51
ρ(kg/L)	0.8301	0.8365	0.8421	0.8275	0.8312	0.8256	0.8324
v at 40 °C (10^{-3}m^2/s)	3.01	3.42	3.88	2.76	3.05	2.42	2.67
LHV (MJ/kg)	42.51	42.28	42.08	39.27	38.93	37.69	37.46
σ(kg/s^2)	0.0275	0.0281	0.02787	0.0262	0.0265	0.0263	0.0268

Table 4 Engine specification for tool validation and numerical results

Parameter	Value
Compression ratio	17.5
Cylinder/type	Single cylinder and 4-stroke
Cooling system	water
Fuel injection timing	23.5º CA b TDC
Fuel spray angle	70˚
Fuel	Diesel, biodiesel
Higher fuel injection pressure	220 bar
Initial pressure	1.0 bar
IV opened/closed	4.51° bTDC/35.51° aBDC
OV opened/closed	35.51° bBDC/4.51° aTDC

Table 5 List of instrument uncertainty

Instrument	Uncertainty (%)
Airflow	±1.0
Crank angle encoder	±0.2
Dynamometer-eddy type	±0.15
Fuel consume indicator	±0.5
FGA	±1
CO_2	±0.5
NO_X	±1.2
CO	
Load meter	±0.2
Pressure transducer	±0.5
Smoke gauge	±1.0
Speed device	±1.0
Temperature detector	±0.15
η_{th}	±0.6
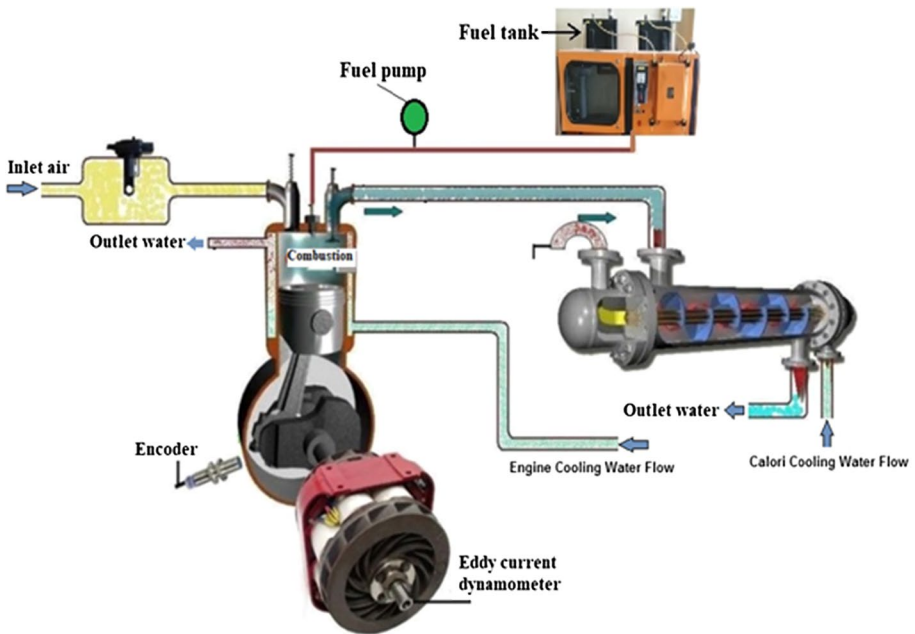
Fig. 2 Complete assemble of experimental setup

$$\%uncertainty = \sqrt{[A_F^2 + \theta^2 + i^2 + F_c^2 + CO_2^2 + NO_x^2 + CO^2 + L^2 + P^2 + Smoke^2 + S^2 + T^2 + \eta^2]}$$

2.3 Model descriptions

Fiveland and Assanis described the following conservations equations in the DRS and, henceforth, they were taken for consideration accordingly (Wei et al., 2018; Fang et al. 2018; Rajak et al., 2019; Zhou et al., 2018; Kuleshov and Mahkamov, 2008; Yu et al., 2018). The following equations describe the species conservation equation, which considers the evaluation and destruction of each species on a mass fraction basis (7–15).

$$\frac{dm}{dt} = \sum j\, \dot{m}_j \tag{7}$$

$$Y_i = \frac{m_i}{m} \tag{8}$$

$$\frac{d(mY_i)}{dt} = \sum j\, \dot{m}_j Y_i^j + \dot{S}_g \tag{9}$$

$$\dot{S}_g = \Omega_i W_{mw} v \tag{10}$$

$$\dot{Y}_i = \sum_j \left(\frac{\dot{m}_i}{m}\right)\left(Y_i^j - Y_i^{cyl}\right) + \frac{\Omega W_{mw}}{\rho} \tag{11}$$

$$\frac{d(mu)}{dt} = -P\frac{dv}{dt} + \frac{dQ_{ht}}{dt} + \sum_j j\, \dot{m}\, h_j \tag{12}$$

$$\alpha_1 = \frac{(A/F)}{(A/F)_s} = \frac{\left(\dot{m}_a/\dot{m}_f\right)}{\left(\dot{m}_a/\dot{m}_f\right)_s} \tag{13}$$

$$FMEP = \alpha + \beta P_{max} + \gamma V_p \tag{14}$$

$$SFC = \frac{\dot{m}_f}{P_b} \tag{15}$$

The aforementioned equation (12) shows that energy is conserved. The rate of change of energy inside the system is indicated on the left-hand side. The rate of displacement work, heat transfer rate, and enthalpy flow are represented by the first, second, and third terms on the right-hand side, respectively. The air-fuel mixture equivalency ratio, denoted by 1, is the ratio of real air/fuel ratio to stoichiometric air/fuel ratio, which is provided in equation (13). As shown in the equation, the frictional mean effective pressure (FMEP) is determined (14). The equation for calculating brake-specific fuel consumption is as follows: (15).

Because the combustion of a fuel in an internal combustion engine occurs in phases, the following governing Eqs. (16-–19) are taken into account in this model and utilised to calculate heat release in the cycle.

- Ignition delay phase period:

The calculating of auto ignition delay period by:

$$3.8 \times 10^{-6} \left(1 - 1.6 \times 10^{-4}. n\right) \sqrt{\frac{T}{p}} \exp\left(\frac{E_a}{8.312T} - \frac{70}{CN + 25}\right) \qquad (16)$$

- Premixed combustion phase period:

Premixed combustion period, the heat release rate by:

$$\frac{dx}{d\tau} = \Phi_0 \times \left(A_0\left(m_f/v_i\right) \times \left(\sigma_{ud} - x_0\right) \times \left(0.1 \times \sigma_{ud} + x_0\right)\right) + \Phi_1 \times \left(\frac{d\sigma_u}{d\tau}\right) \qquad (17)$$

- Mixing controlled combustion phase period:

In mixing controlled combustion phase period, the heat release rate can be given by:

$$\frac{dx}{d\tau} = \Phi_1 \times \left(\frac{d\sigma_u}{d\tau}\right) + \Phi_2 \times \left(A_2\left(m_f/v_c\right) \times \left(\sigma_u - x\right) \times (\alpha - x)\right) \qquad (18)$$

- Late burning phase period:

In this phase period, the heat release rate is given by:

$$\frac{dx}{dt} = \phi_3 A_3 K_T (1 - x)(\xi_b \alpha - x) \qquad (19)$$

In these four phase period equation is given Q0 = Q1 = Q2 = Q3 = Constants which function describe the completeness of fuel vapor combustion in this phase period.

The chain Zeldovich technique is used to determine the thermal NO, as shown in Eqs. (20–23). Every step calculates the equilibrium concentrations of eighteen species, and the entire system of equations incorporates fourteen equilibrium equations, three material balance equations, and the Dalton partial pressure Eq.

$$O_2 \leftrightarrow 2O, N_2 + O \leftrightarrow NO + O, N + O_2 \leftrightarrow NO + O \qquad (20)$$
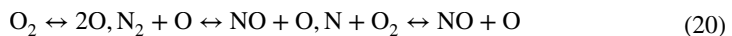
$$\frac{d[NO]}{d\theta} = \frac{P \times 2.333 \times 10^{-7}.e^{-\frac{38,020}{T_b}} [N_2]_e.[O]_e.\left\{1 - \left([NO]/[NO]_e\right)^2\right\}}{R.T_b.\left(1 + \frac{2365}{T_b}.e^{\frac{2365}{T_b}}.\frac{[NO]}{[NO]_e}\right)}.\frac{1}{\omega} \qquad (21)$$

The NO concentration in a cylinder is given by:

$$r_{NO_c} = r_{NO} \qquad (22)$$

And the specific NO in g/kWh is expressed as

$$e_{\text{NO}} = \frac{30 \times r_{\text{NO}} \times M_{\text{bg}}}{L_{\text{C}} \times \eta_{\text{M}}} \tag{23}$$

Soot formation.

Unburned hydrocarbons cause soot to form in diesel engines, posing a serious health risk and polluting the environment. The Hatridge smoke level, which is given in the equation, can be used to calculate the level of soot generation (24-25). The equation is used to calculate the generation of soot in the burning zone.

$$\left(\frac{d[C]}{dt}\right)_{\text{K}} = 0.004 \frac{q_{\text{c}}}{V} \frac{dx}{dt} \tag{24}$$

$$\text{Hartridge} = 100\{1 - 0.9545\exp(-2.4226[C])\} \tag{25}$$

The following equation (26) is used by the Diesel-RK programme to calculate particulate matter as a function of Bosch number.

$$[\text{PM}] = Z_{\text{PM}}565\left(\ln\frac{10}{10-\text{BN}}\right)^{1.206} \tag{26}$$

In equation (26) Z_{PM} is a constant equal to 1.

2.4 Validation

Diesel, SMAB and its different blends with the alcohols are used for numerical investigations of engine characteristics through DRS. From A reasonable accuracy was found between experiment and simulation values (Figs. 3 and 4). Minor error deviations are subjected to the conditions between experimental and simulation assumptions. The error Error deviation found in the current investigation was 3.28% for pressure and 1.53% for in-heat dissipation rate with crank angle. Cylinder pressure and heat liberation rate are same
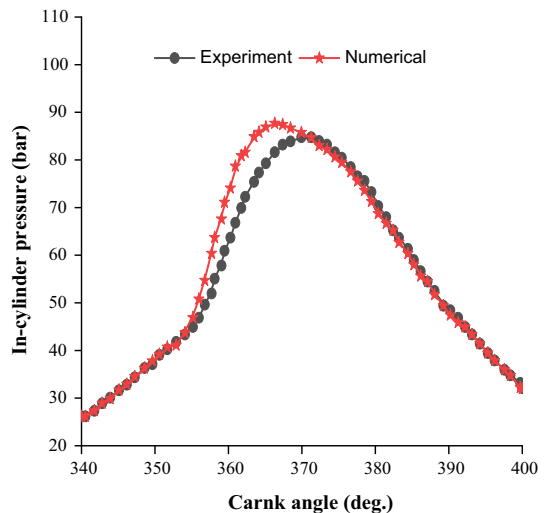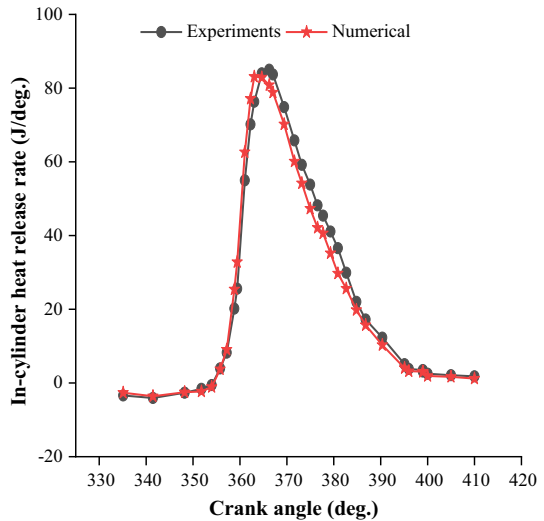
Fig. 3 Pressure with crank angle

Fig. 4 Cylinder heat release rate with crank angle

for all operating conditions, as shown in Table 3. Necessary validation is done for engine parameters such as cylinder pressure and heat liberation rate using diesel fuel through Diesel-RK tool. However, at a higher load state (100%), the variance between the numerical and investigational value of pressure of cylinder enhanced. Heat liberation rate decreased whose values are noted to be in-cylinder pressure (Experimental – 85.3 bar and Numerical – 88.2 bar) and in-cylinder heat release rate (Experimental 85.2 J/deg. and Numerical – 83.9 J/deg.), respectively.

Fig. 5 Brake specific fuel consumption with engine loads
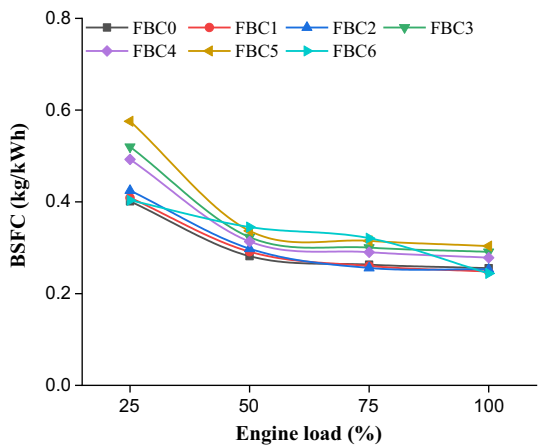
3 Results and discussion

3.1 Performance characteristics

The value of BSFC of FBC0, FBC1, FBC2, FBC3, FBC4, FBC5, and FBC6 blends with the various loads of engine are indicated in Fig. 5. An increasing percentage of SMAB, ethanol, and menthol in the blends reduced the viscosity and surface tension of the blends. In this study, the use of ethanol and methanol blending with diesel-SMAB up to 20% volume-based is investigated. BSFC is lower at higher engine loads for all tested fuel blends with constant engine parameters. Also, it can be noted that during high loads, the quantity of supplied fuel inside the cylinder increases while available oxygen for combustion reduces (Abdalla. A. N., 2019, 2020). Thus, the air-fuel ratio is changed, which increases the BSFC. When the SMAB fuel blending percentage increases to 40% from 0.0% at higher engine load, the fuel consumption increases to 4.0% compared with diesel fuel. At higher loads, an increase in the alcohol (ethanol) increases the fuel consumption by 17.2% than that of diesel fuel. Due to the higher percentage of oxygen and LCV of alternative fuel than diesel fuel, both the fuel (SMAB and alcohol) percentage increases in the blend and the fuel consumption increase. The value of BSFC for FBC0, FBC1, FBC2, FBC3, FBC4, FBC5 and FBC6 was obtained to be 0.24, 0.25, 0.253, 0.29, 0.278, 0.31, and 0.224 kg/kWh, respectively, at 100% load.

BTE of FBC0, FBC1, FBC2, FBC3, FBC4, FBC5, and FBC6 blends with the variation of loads on the engine are shown in Fig. 6. Percentage increase of biodiesel, ethanol, and menthol in the blends diminished the calorific value of the blend in FBC0, FBC1, FBC2, FBC3, FBC4, FBC5, and FBC6. 20% volume-based ethanol and methanol blend with diesel-microalgae biodiesel is considered in the present work. BTE is higher at higher engine load for all tested fuel blends with constant engine parameters. Cylinder temperature enhances with rise in engine load and improved combustion.

BTE is evaluated and compared to diesel fuel at higher loads. When SMAB fuel blending percentage is increased to 40%, brake thermal efficiency reduces by 3.4%. With rise in alcohol fuel (ethanol) at maximum engine load, BTE declines by 1.3% than that of FBC0. Decrease in BTE is observed as alcohol and biodiesel are increased in the blends. For FBC0, FBC1, FBC2, FBC3, FBC4, FBC5, and FBC6, BTE follows similar trend to that of

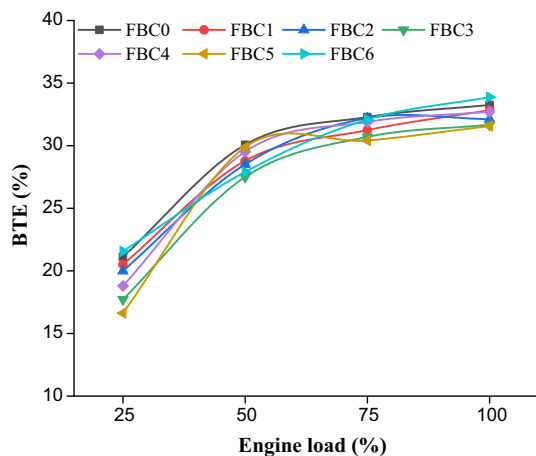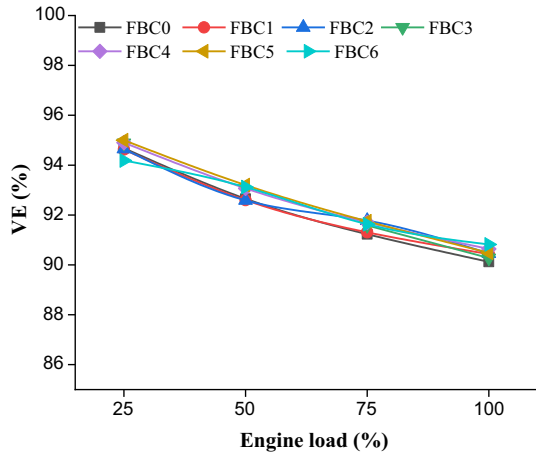**Fig. 6** Brake thermal efficiency under different engine loads for various blends

Fig. 7 Volumetric efficiency under different engine loads for various blends

FBC0. Since CV of alternative fuel is lesser than base fuel, both fuel *(spirulina microalgae and alcohol)* percentage increases in the blend and the BTE decreases. Yet, it was observed to be higher for FBC6 (80% of FBC2 and 20% of methanol). BTE for FBC0, FBC1, FBC2, FBC3, FBC4, FBC5, and FBC6 was obtained to be 33.25, 32.83, 32.1, 31.6, 32.7, 31.5, and 33.8%, respectively, at 100% load. The FBC6 shows higher BTE because of addition of oxygenates and low heating value of fuel.

Volumetric efficiency of FBC0, FBC1, FBC2, FBC3, FBC4, FBC5, and FBC6 blends with the change in engine loads are depicted in Fig. 7. Percentage rise of biodiesel and alcohols in the blends reduces the viscosity and surface tension of the blend in FBC0, FBC1, FBC2, FBC3, FBC4, FBC5, and FBC6. This study uses ethanol and methanol blending with diesel-microalgae biodiesel up to 20% volume-based. Volumetric efficiency is maximum at lesser engine load and minimum at high engine loads for all fuel blends with constant engine parameters. Figure 7 of volumetric efficiency shows that at higher engine load when the SMAB fuel blending percentage increases to 40%, the volumetric efficiency increases to 4.0% compared to base fuel.

Fig. 8 Cylinder peak pressure with engine loads
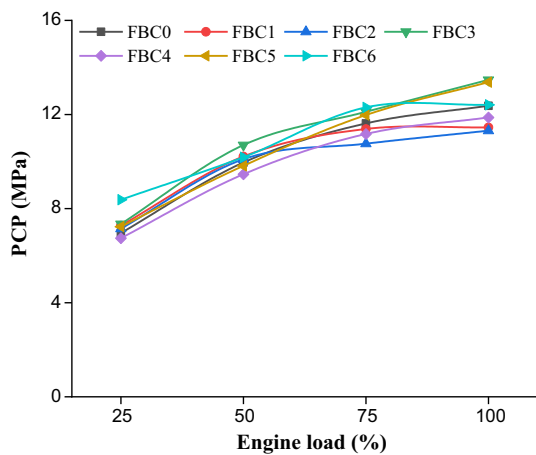
At high engine load, with the rise of alcohol (ethanol) in the fuel, volumetric efficiency enhances to 0.36% (FBC4) than diesel fuel (FBC0). Higher percentage of oxygen and lower calorific value of alternative fuel than that of base fuel, both the fuel (SMAB and alcohol) percentage increases in the blend and the volumetric efficiency enhance. The value of volumetric efficiency for FBC0, FBC1, FBC2, FBC3, FBC4, FBC5, and FBC6 was obtained to be 90.1, 90.4, 90.45, 90.2, 90.64, 90.5, and 90.8%, respectively, at 100% load.

The value of PCP of FBC0, FBC1, FBC2, FBC3, FBC4, FBC5, and FBC6 blends with the change in engine loads is engine loads shown in Fig. 8. A percentage increase of biodiesel, ethanol, and menthol in the blends reduced the calorific value of the blend in FBC1, FBC2, FBC3, FBC4, FBC5, and FBC6. PCP is higher at high engine load for all considered fuel blends with constant engine parameters. PCP rises with a rise in engine load and improved combustion (Rajesh et al., 2015; Rajak et al., 2019). From Fig. 8, PCP is obtained and compared to base fuel at high loads; when the SMAB fuel blending percentage increases to 40%, the PCP reduces by 8.64% (FBC3) as compared to FBC0. With the rise in the alcohol (methanol) at high engine load, the PCP enhances to 7.47% (FBC5) than FBC0. Cylinder pressure increases as alcohol (methanol) increase in the blends. Due to the lesser CV of alternative fuel than diesel, the SMAB fuel percentage enhances the blend and the cylinder pressure decreases. PCP for FBC0, FBC1, FBC2, FBC3, FBC4, FBC5, and FBC6 was obtained to be 12.37, 11.44, 11.3, 13.47, 11.87, 13.37, and 12.41 MPa, respectively, at 100% load.

3.2 Spray characteristics

DOD of FBC0, FBC1, FBC2, FBC3, FBC4, FBC5, and FBC6 blends with the engine loads are shown in Fig. 9. The percentage rise of biodiesel, ethanol, and menthol in the blends reduced the FBC1, FBC2, FBC3, FBC4, FBC5, and FBC6 blends calorific value. DOD is higher at less engine load for all considered fuel blends for the engine. DOD diminishes with the rise in load of the engine and due to improved combustion (Qi et al. 2019). Figure 9 shows the variation of DOD at all loads for each blend, when the SMAB fuel blending percentage enhances to 40% the DOD improves by 11.9% (FBC2) as compared to FBC0. With the rise in the alcohol (methanol) at higher engine load, DOD decreases to 3.1% (FBC5) than FBC0. For FBC1, FBC2, FBC3, FBC4, FBC5, and FBC6, the DOD

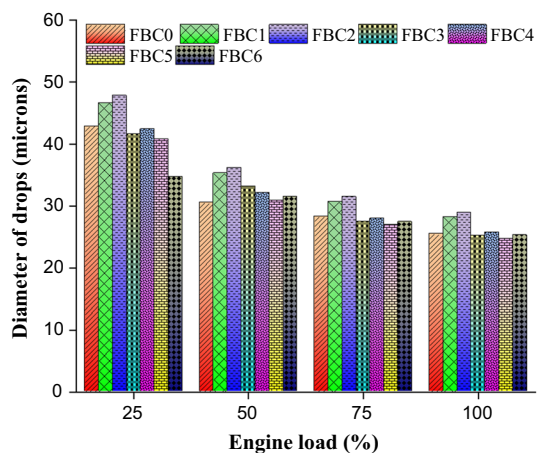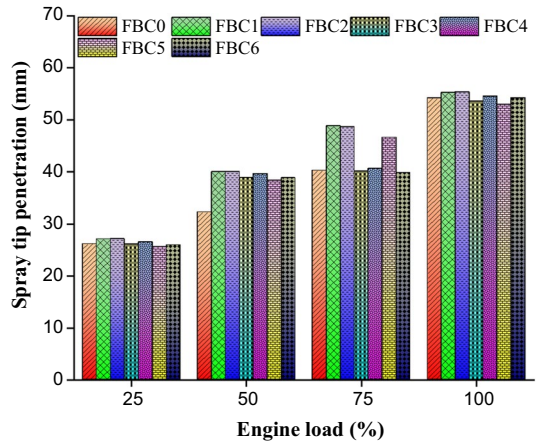**Fig. 9** Diameter of drops with engine loads

**Fig. 10** Diameter of drops with engine loads

is similar to FBC0. Due to surface tension and viscosity value of alternative fuel, the fuel (SMAB) percentage rise in the blend and the diameter of drops is enhanced. The value of DOD for FBC0, FBC1, FBC2, FBC3, FBC4, FBC5, and FBC6 was obtained to be 25.47, 28.22, 28.94, 25.21, 25.72, 24.7, and 25.26 microns, respectively, at 100% load.

FSTP of FBC0, FBC1, FBC2, FBC3, FBC4, FBC5, and FBC6 blends with change in loads of engine are shown in Fig. 10. Percentage increase of biodiesel, ethanol, and menthol in the blends diminished the viscosity of the FBC1, FBC2, FBC3, FBC4, FBC5, and FBC6 blends as compared to pure SMAB. The FSTP is higher at higher engine load for all considered fuel blends in the present study. FSTP rises with the rise in engine load and aerodynamic resistance of the ambient gas and kinetic energy (Qi DH et al., 2019). From Fig. 10 it can be observed that when the SMAB fuel blending percentage is increased to enhance to 40% FSTP improves by 2.18% (FBC2) as compared to FBC0. The increase in the alcohol decreases FSTP of the blend fuels compared to FBC0 at higher engine loads.

An increase in FSTP is observed as SMAB percentage in the blends increases. For FBC1, FBC2, FBC3, FBC4, FBC5, and FBC6, FSTP are similar to FBC0. It is due to kinetic energy of alternative fuel, fuel SMAB percentage increases in blend and diameter

Fig. 11 Spray cone angle with engine loads
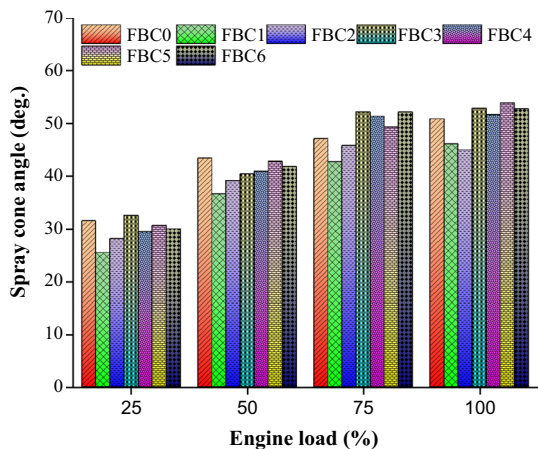
of drops are also increased. FSTP for FBC0, FBC1, FBC2, FBC3, FBC4, FBC5, and FBC6 was obtained to be 54.1, 55.2, 55.28, 53.55, 54.48, 52.89, and 54.17 mm, respectively, at 100% load. The 40% of SMAB has the longest FSTP and 20% of SMAB with 20% of methanol has the shortest, nearly comparable to that of 100% diesel. Ambient gas density and blends density are the key features that affect FSTP before and after splitting the liquid column, thus injected (Rajak et al., 2020).

SCA of FBC0, FBC1, FBC2, FBC3, FBC4, FBC5, and FBC6 blends with the engine loads are shown in Fig. 11. With increasing percentage of SMAB in blends (FBC1 and FBC2), SCA is reduced due to higher viscosity and momentum, however, adding ethanol and menthol to SMAB blends are improved for FBC3, FBC4, FBC5 and FBC6 as compared to FBC0 due to lower viscosity and momentum. SCA is higher at higher engine load for all considered fuel blends in the present study. SCA enhances with a rise in engine load and due to the momentum of fuel (Qi et al., 2019). From Fig. 11, SCA is obtained compared to base fuel at all loads, when the SMAB fuel blending percentage increases to 40%, the SCA is reduced by 11.61% (FBC2) as compared to FBC0. With the increase in alcohol in fuel at higher engine load, the SCA improved by 5.4% (FBC5) than FBC0.

Decrease in SCA is observed as SMAB percentage in the blends (FBC1 and FBC2). While the higher for FBC3, FBC4, FBC5, and FBC6, the SCA is similar to FBC0. Due to the high viscosity and momentum of alternative fuel, the fuel (SMAB) percentage rises in the blend and the SCA is enhanced. SCA for FBC0, FBC1, FBC2, FBC3, FBC4, FBC5, and FBC6 was obtained to be 50.88 46.2, 44.97, 52.8, 51.6, 53.8, and 52.7 degree, respectively, at 100% load. 40% of SMAB has shortest spray cone angle and 20% of SMAB with 20% of methanol the longest, which is nearly comparable to that of 100% of diesel. The fuel injection pressure, viscosity, and momentum of blends are the key features affecting SCA (Qi et al., 2019).
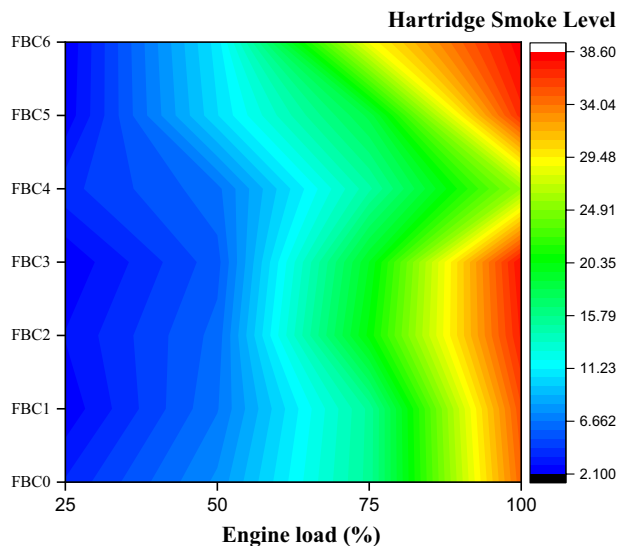

Fig. 12 NO_X emission with engine loads
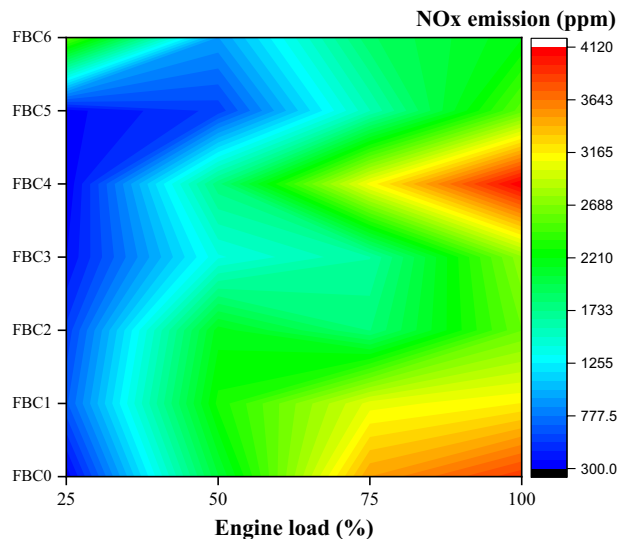
3.3 Emission characteristics

NOx emissions are produced when diatomic nitrogen is divided into a single nitrogen molecule, which then bonds with oxygen molecules at high temperatures. As a result, as the temperature and oxygen content in the cylinder rise, the NOx emission rises. The typical trend is for NOx emissions to rise with engine load as the in-cylinder gas temperature rises. Diesel produces the highest quantities of NOx at each engine loading, whereas ethanol produces the lowest levels (Ağbulut U et al., 2020).

NO_X emissions of FBC0, FBC1, FBC2, FBC3, FBC4, FBC5, and FBC6 combination fuels with engine loads are shown in Fig. 12. Percentage rise in SMAB, ethanol, and methanol in the blends (FBC1 FBC2, FCB3, FBC5, and FBC6), NO_X emissions is diminished due to improve combustion and higher contents of oxygen in the mixture compared to FBC0. The influence of SMAB and alcohol fuel blends on the NO_X emissions of the engine is depicted in Fig. 12. The NO_X emission is maximum at high engine load for all considered fuel blends in the present study. The NO_X emissions enhance with the rise in engine loads and increase combustion temperature (Chang KL et al., 2019). From Fig. 12, NO_X emissions are obtained for the SMAB fuel blending percentage rises to 40% from 0%, NO_X emissions diminished by 32.6% (FBC2) as compared to FBC0. With the rise in the alcohol fuel in the blends at high engine loads, the NO_X emissions reduced by 43.1% (FBC6) than FBC0.

Decrease in NO_X emissions is observed as SMAB percentage in the blends (FBC1 and FBC2). While the higher for FBC4, the NO_X emissions are similar to that of FBC0. Due to more oxygen content of SMAB, fuel (SMAB) percentage increases in the blend and NO_X emissions are decreased. NO_X emissions for FBC0, FBC1, FBC2, FBC3, FBC4, FBC5, and FBC6 was obtained to be 3867.1, 3168.1, 2604.9, 2753.0, 4119.4, 2575.8, and 2201.4 ppm, respectively, at 100% load. The combination of FBC6 has the shortest NO_X emissions and the combination of FBC4 the longest, which is nearly equivalent to that of 100% of base fuel diesel. Fuel combustion temperature, engine

**Fig. 13** Hartridge smoke level with engine loads

loads, and combinations of fuel are key features affecting NO_X emissions (Rajak et al., 2020).

HSL emissions of FBC0, FBC1, FBC2, FBC3, FBC4, FBC5, and FBC6 combination fuels with the engine loads are shown in Fig. 13. Rise in engine loads. HSL emissions are being enhanced for a percentage of the rise of SMAB, ethanol, and menthol in the blends (FBC1 FBC2, FCB3, FBC5, and FBC6). HSL emission is diminished due to improved combustion temperature and penetration length for FBC4 as that to FBC0. Effect of SMAB and alcohol fuel blends on the HSL emissions of the CI engine rig is depicted in same figure. HSL emission is maximum at high engine load for all fuel blends in the current study. HSL emissions increase with the rise in engine load due to increased combustion temperature (Chang et al., 2019; Kuleshov et al., 2008). From Fig. 13, HSL emissions are obtained, as compared to diesel fuel at loads, when the SMAB fuel blending percentage rises to 40% from 0%, the HSL emissions increased by 7.2% (FBC2) as compared to FBC0. With the rise in the alcohol fuel in the blends at high engine load, the HSL emissions enhanced but diminished by 25.7% for FBC4 than FBC0.

The value of HSL emissions for FBC0, FBC1, FBC2, FBC3, FBC4, FBC5, and FBC6 was obtained to be 34.6, 35.47, 37.26, 37.95, 34.2, 36.8, and 38.51, respectively, at 100% load. The FBC4 has lowest HSL emissions whereas FBC6 has highest which is nearly comparable to that of 100% of diesel. The fuel combustion temperature, engine loads, and oxygen content key feature affecting HSL emissions (Rajak et al., 2019; Kuleshov et al. 2008). Smoke is produced as a result of incomplete combustion, which is caused by a lack of oxygen in the combustion chamber as well as the existence of a fuel-rich zone at the time of combustion. The amount of smoke produced by an engine increases as the load increases, owing to the increased fuel consumption. Among the tested fuels, diesel produces the most smoke, while ethanol produces the least. The lower ethanol smoke level can be due to the increased oxygen concentration that leads to complete combustion.

SOE of blends (FBC0, FBC1, FBC2, FBC3, FBC4, FBC5, and FBC6) with the engine loads are depicted in Fig. 14. Percentage enhancement of SMAB in the blends

Fig. 14 Summary of emission with engine loads
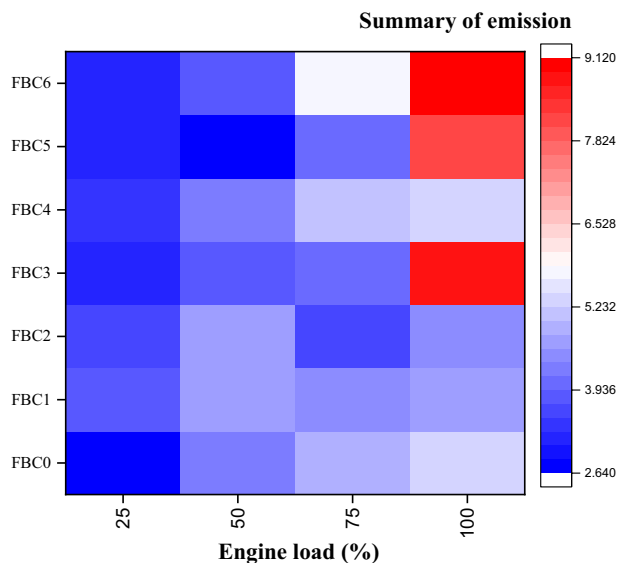
(FBC1 and FBC2) diminishes the SOE due to better combustion and oxygen. When ethanol and menthol are added to SMAB and diesel blends, SOE is higher for FBC3, FBC4, FBC5 and FBC6 than FBC0 due to cooling effect. The SOE is high at higher engine load conditions for all fuel blends in the present study. SOE increases with an escalation in engine load due to high combustion temperature and better combustion (Petranovi et al., 2017; Singh et al., 2021; Yildiz I et al., 2019). From Fig. 14, SOE is lower for SMAB fuel blending percentage increases to 40% from 0%. SOE is reduced by 15.54% (FBC2) as compared to FBC0. With the increase in the alcohol fuel in the blends at high engine load, the SOE improved by 41.38% (FBC6) than FBC0. The value of SE for FBC0, FBC1, FBC2, FBC3, FBC4, FBC5, and FBC6 was 5.34 4.72, 4.51, 8.72, 5.33, 8.22, and 9.11, respectively, at full load. At maximum engine load, overall emissions for FBC2 (4.51) are 15.54% lower than for FBC0 (diesel fuel), owing to the existence of an additional oxygen molecule bound to the hydroxyl atom, which supplies more oxygen to the rich fuel zone and hence minimises emission formation compared to diesel fuel.

4 Conclusions

A numerical simulation was carried to examine the influence of SMAB-ethanol-methanol- diesel fuel blends on a CI engine's spray properties, performance, and tailpipe emissions. From the numerical simulation results, the subsequent conclusions are drawn:

- Viscosity and density of SMAB were diminished by blending it with ethanol, methanol, and diesel fuels.
- Percentage increase of SMAB to 40% in diesel-biodiesel blends elevated the diameter of drops by 11.9% and free-spray tip penetration by 5.4%. It lessened the spray-cone angle by 11.6% due to the higher viscosity.
- Percentage increase of alcohol in diesel-biodiesel blends diminished the diameter of drops and free-spray tip penetration but enhanced the spray-cone angle due to adverse effects.
- Blend FBC6 fuel showed elevated brake thermal efficiency by 1.6% and lesser fuel consumption for the rig. Enhancing percentage of alcohol in diesel - biodiesel blends decreases the nitrogen oxide emission by 43%, while the Hartridge smoke level shows an opposite tendency.

For blend FBC4 fuel lesser summary of emissions is obtained than that of other blends at 100% load. This investigation can promote a compression ignition engine and reassure the usage of this new kind of blend of ethanol and methanol with third-generation spirulina microalgae biodiesel.

Author contribution Upendra Rajak: Writing original draft. Abhishek Dasore: Resources & Supervision. Prem Kumar Chaurasiya: Resources & Supervision.Tikendra Nath Verma: Editing the Manuscript.Prerana Nashine: Editing the Manuscript.Anil Kumar: Reviewing & final drafting.

Declarations

Conflict of interest The authors declare that they have no known competing financial interests or personal relationships that could have appeared to influence the work reported in this paper.

References

An, H., Yang, W. M., & Li, J. (2015). Effects of ethanol addition on biodiesel combustion: A modeling study. Applied Energy, 143, 176–188. https://doi.org/10.1016/j.apenergy.2015.01.033

Ahmed, N., Abdalla, A. N., Hai, T., Bagaberc, S. A., Alid, O. M., Kamile, M. … Awad, O. I. (2019). Prediction of emissions and performance of a gasoline engine running withfusel oil–gasoline blends using response surface methodology. Fuel, 253, 1–14. https://doi.org/10.1016/j.fuel.2019.04.085

Abdalla, A. N., Bakara, R. A., Tao, H., Ramasamy, D., Kadirgama, K., Fooj, B. … Sivaraos, S. (2020). Effect of swirl at intake manifold on engine performance using ethanol fuel blend. Energy Sources, Part A: Recovery, Utilization, and Environmental Effects, 42(1), 73–83. https://doi.org/10.1080/15567036.2019.1587056

Ağbulut, Ü., Sarıdemir, S., & Karagöz, M. (2020). Experimental investigation of fusel oil (Isoamyl alcohol) and diesel blends in a CI engine. Fuel, 267, 117042. https://doi.org/10.1016/j.fuel.2020.117042

Balasubramanian R, Subramanian KA (2019) Experimental investigation on the effects of compression ratio on performance, emissions and combustion characteristics of a biodiesel-fueled automotive diesel engine. Biofuels. https://doi.org/10.1007/s11356-019-04649-6

Çelebi, Y., & Ayd, H. (2019). An overview on the light alcohol fuels in diesel engines. Fuel, 236, 890–911. https://doi.org/10.1016/j.fuel.2018.08.138

Chen, C., Yao, A., Yao, C., Wang, B., Lu, H., Feng, J., & Feng, L. (2019). Study of the characteristics of PM and the correlation of soot and smoke opacity on the diesel methanol dual fuel engine. Applied Thermal Engineering, 148(92), 391–403. https://doi.org/10.1016/j.applthermaleng.2018.11.062

Chang, K. L., Amesho, K. T. T., Lin, Y. C., Jhanga, S. R., Chou, F. H., & Chen, H. C. (2019). Effects of atmospheric-plasma system on energy efficiency improvement and emissions reduction from a diesel engine. Journal of Environmental Management, 234, 336–344. https://doi.org/10.1016/j.jenvman.2019.01.017

Datta, A., & Mandal, B. K. (2017). Engine performance, combustion and emission characteristics of a compression ignition engine operating on different biodiesel-alcohol blends. Energy, 125, 470–483. https://doi.org/10.1016/j.energy.2017.02.110

Fang, Q., Fang, J., Zhuang, J., & Huang, Z. (2013). Effects of ethanol-diesel-biodiesel blends on combustion and emissions in premixed low temperature combustion. Applied Thermal Engineering, 54(2), 541–548. https://doi.org/10.1016/j.applthermaleng.2013.01.042

Ghadikolaei, M. A., Cheung, C. S., & Yung, K. F. (2018). Study of combustion, performance and emissions of diesel engine fueled with diesel/biodiesel/alcohol blends having the same oxygen concentration. Energy, 157, 258–269. https://doi.org/10.1016/j.energy.2018.05.164

Ghadikolaei, M. A., Cheung, C. S., & Yung, K. F. (2019). Comparison between blended mode and fumigation mode on combustion, performance and emissions of a diesel engine fueled with ternary fuel (diesel-biodiesel-ethanol) based on engine speed. Journal of the Energy Institute, 92(5), 1233–1250. https://doi.org/10.1016/j.joei.2018.10.010

Gopidesi, R. K., Sr, P., & Dhana Raju, V. (2021). Mitigation of harmful exhaust pollutants of DI diesel engine using emulsified fuel and hythane gas in a dual-fuel mode. Energy Sources, Part A: Recovery, Utilization, and Environmental Effects. Jan 2:1–23. https://doi.org/10.1080/15567036.2020.1861131

Hoseini, S. S., Najafi, G., Ghobadian, B., Mamat, R., Sidik, N. A. C., & Azmi, W. H. (2017). The effect of combustion management on diesel engine emissions fueled with biodiesel-diesel blends. Renewable and Sustainable Energy Reviews, 73, 307–331. https://doi.org/10.1016/j.rser.2017.01.088

Jiang, Z., Gan, Y., Ju, Y., Liang, J., & Zhou, Y. (2019). Experimental study on the electrospray and combustion characteristics of biodiesel-ethanol blends in a meso-scale combustor. Energy, 179, 843–849. https://doi.org/10.1016/j.energy.2019.05.024

Jiao, Y., Liu, R., Zhang, Z., Yang, C., Zhou, G., Dong, S., & Liu, W. (2019). Comparison of combustion and emission characteristics of a diesel engine fueled with diesel and methanol-Fischer-Tropsch diesel-bio-diesel-diesel blends at various altitudes. Fuel, 243, 52–59. https://doi.org/10.1016/j.fuel.2019.01.107

Kuszewski, H. (2019). Experimental investigation of the auto ignition properties of ethanol–biodiesel fuel blends. Fuel, 235, 1301–1308. https://doi.org/10.1016/j.fuel.2018.08.146

Krishna, S. M., Abdul, S. P., Tongroon, M., & Chollacoop, N. (2019). Performance and emission assessment of optimally blended biodiesel-diesel-ethanol in diesel engine generator. Applied Thermal Engineering, 155, 525–533. https://doi.org/10.1016/j.applthermaleng.2019.04.012

Khoobbakht, G., Karimi, M., & Kheiralipour, K. (2019). Effects of biodiesel-ethanol-diesel blends on the performance indicators of a diesel engine: A study by response surface modeling. Applied Thermal Engineering, 148, 1385–1394. https://doi.org/10.1016/j.applthermaleng.2018.08.025

Kandasamy, S. K., Selvaraj, A. S., & Rajagopal, T. K. R. (2019). Experimental investigations of ethanol blended biodiesel fuel on automotive diesel engine performance, emission and durability characteristics. Renewable Energy, 141, 411–419. https://doi.org/10.1016/j.renene.2019.04.039

Kuleshov, A., & Mahkamov, K. (2008). Multi-zone diesel fuel spray combustion model for the simulation of a diesel engine running on biofuel. Proceedings of the Institution of Mechanical Engineers, Part A: Journal of Power and Energy, 222(3), 309–321. https://doi.org/10.1243/09576509JPE530.

Laraib, N., Manzoor, M., Javid, A., Jabeen, F., Bukhari, S. M., Ali, W., & Hussain, A. (2021). Mixotrophic cultivation of Chlorella vulgaris in sugarcane molasses preceding nitrogen starvation: biomass productivity, lipid content, and fatty acid analyses. Environmental Progress & Sustainable Energy, 12: e13625. https://doi.org/10.1002/ep.13625.

Laraib, N., Hussain, A., Javid, A., Bukhari, S. M., Ali, W., Manzoor, M., & Jabeen, F. (2021). Mixotrophic cultivation of scenedesmus dimorphus for enhancing biomass productivity and lipid yield. Iranian Journal of Science and Technology, Transactions A: Science, 45(2), 397–403. https://doi.org/10.1007/s40995-020-01055-3.

Mofijur, M., Rasul, M. G., Hyde, J., Azad, A. K., Mamat, R., & Bhuiya, M. M. K. (2016). Role of biofuel and their binary (diesel-biodiesel) and ternary (ethanol-biodiesel-diesel) blends on internal combustion engines emission reduction. Renewable and Sustainable Energy Reviews, 53, 265–278. https://doi.org/10.1016/j.rser.2015.08.046

Park, S. H., Suh, H. K., & Lee, C. S. (2010). Nozzle flow and atomization characteristics of ethanol blended biodiesel fuel. Renewable Energy, 35(1), 144–150. https://doi.org/10.1016/j.renene.2009.06.012

Petranovi, Z., Seni, T. B., Vujanovi, M., & Dui, N. (2017). Modelling pollutant emissions in diesel engines, influence of biofuel on pollutant formation. Journal of Environmental Management, 203(3), 1038–1046. https://doi.org/10.1016/j.jenvman.2017.03.033

Qi, D. H., Ding, X. Q., Zhao, W. B., & Yang, K. (2019). Spray characteristics and engine performance of vegetable oil-diesel-ethanol hybrid fuel. Journal of Energy Engineering, 145(4), 1–8. https://doi.org/10.1061/(ASCE)EY.1943-7897.0000606

Rajak, U., Nashine, P., Verma, T. N., & Pugazhendhi, A. (2019). Alternating the environmental benefits of Aegle-diesel blends used in compression ignition. Fuel, 256, 115835. https://doi.org/10.1016/j.fuel.2019.115835

Rajak, U., Nashine, P., Verma, T. N., & Pugazhendhi, A. (2019). Performance, combustion and emission analysis of microalgae spirulina in a common rail direct injection diesel engine. Fuel, 255, 115855. https://doi.org/10.1016/j.fuel.2019.115855

Rajak, U., Nashine, P., & Verma, T. N. (2019). Assessment of diesel engine performance using spirulina microalgae biodiesel. Energy, 166, 1025–1036. https://doi.org/10.1016/j.energy.2018.10.098

Rajak, U., Nashine, P., & Verma, T. N. (2019). Characteristics of microalgae spirulina biodiesel with the impact of n-butanol addition on a CI engine. Energy, 189, 116311. https://doi.org/10.1016/j.energy.2019.116311

Rajesh, K. B., & Saravanan, S. (2015). Effect of exhaust gas recirculation (EGR) on performance and emissions of a constant speed di diesel engine fueled with pentanol/diesel blends. Fuel, 160, 217–226. https://doi.org/10.1016/j.fuel.2015.07.089

Rajak, U., Nashine, P., & Verma, T. N. (2019). Experimental study on spray characteristics of biodiesel-diesel fuels blends In a constant volume chamber. Journal of Engineering and Applied Sciences, 5(2), 1–12

Rajak, U., Nashine, P., Verma, T. N., & Pugazhendhi, A. (2020). Performance and emission analysis of a diesel engine using hydrogen enriched n-butanol, diethyl ester and Spirulina microalgae biodiesel. Fuel, 271, 117645. https://doi.org/10.1016/j.fuel.2020.117645

Raman, L. A., Deepanraj, B., Rajakumar, S., & Sivasubramanian, V. (2019). Experimental investigation on performance, combustion and emission analysis of a direct injection diesel engine fuelled with rapeseed oil biodiesel, Fuel. 246:69–74. https://doi.org/10.1016/j.fuel.2019.02.106

Ranjitha, J., Gokul Raghavendra, S., Vijayalakshmi, S., & Deepanraj, B. (2020). Production, optimisation and engine characteristics of beef tallow biodiesel rendered from leather fleshing and slaughterhouse wastes. Biomass Conversion and Biorefinery, 10(3), 675–688. https://doi.org/10.1007/s13399-019-00501-6.

Shamun, S., Belgiorno, G., Blasio, D. G., Beatrice, C., & Tunestål, T. M., P (2018). Performance and emissions of diesel-biodiesel-ethanol blends in a light duty compression ignition engine. Applied Thermal Engineering, 145, 444–452. https://doi.org/10.1016/j.applthermaleng.2018.09.067

Sun, X., Liang, X., Shu, G., Lin, J., Wang, Y., & Wang, Y. (2017). Numerical investigation of two-stroke marine diesel engine emissions using exhaust gas recirculation at different injection time. Ocean Engineering, 144, 90–97. https://doi.org/10.1016/j.oceaneng.2017.08.044

Sahar, Sadaf, S., Iqbal, J., Ullah, I., Bhatti, H. N., Nouren, S., & Iqbal, M. (2018). Biodiesel production from waste cooking oil: An efficient technique to convert waste into biodiesel. Sustainable Cities and Society, 41, 220–226. https://doi.org/10.1016/j.scs.2018.05.037

Singh, T. S., Rajak, U., Dasore, A., Muthukumar, M., & Verma, T. N. (2021). Performance and ecological parameters of a diesel engine fueled with diesel and plastic pyrolyzed oil (PPO) at variable working parameters. Environmental Technology & Innovation, 22: 101491.

Saleem, A., Hussain, A., Chaudhary, A., Ahmad, Q. U., Iqtedar, M., Javid, A., & Akram, A. M. (2020.) Acid hydrolysis optimization of pomegranate peels waste using response surface methodology for ethanol production. Biomass Conversion and Biorefinery. 1–2. https://doi.org/10.1007/s13399-020-01117-x

Tutak, W., Jamrozik, A., Pyrc, M., & Sobiepański, M. (2017). A comparative study of co-combustion process of diesel-ethanol and biodiesel-ethanol blends in the direct injection diesel engine. Applied Thermal Engineering, 117, 155–163. https://doi.org/10.1016/j.applthermaleng.2017.02.029

Thiyagarajan, S., Varuvel, E. G., Martin, L. J., & Beddhannan, N. (2019). Mitigation of carbon footprints through a blend of biofuels and oxygenates, combined with post-combustion capture system in a single cylinder CI engine. Renewable Energy, 130, 1067–1081. https://doi.org/10.1016/j.renene.2018.07.010

Wei, L., Cheung, C. S., & Ning, Z. (2018). Effects of biodiesel-ethanol and biodiesel-butanol blends on the combustion, performance and emissions of a diesel engine. Energy, 155, 957–970. https://doi.org/10.1016/j.energy.2018.05.049

Yu, S., Yin, B., Deng, W., Jia, H., Ye, Z., Xu, B., & Xu, H. (2018). Internal flow and spray characteristics for elliptical orifice with large aspect ratio under typical diesel engine operation conditions. Fuel, 228, 62–73. https://doi.org/10.1016/j.fuel.2018.04.156

Yildiz, I., Açıkkalp, E., Caliskan, H., & Morid, K. (2019). Environmental pollution cost analyses of biodiesel and diesel fuels for a diesel engine. Journal of Environmental Management, 243, 218–226. https://doi.org/10.1016/j.jenvman.2019.05.002

Zhou, X., Li, T., Lai, Z., & Wang, B. (2018). Scaling fuel sprays for different size diesel engines. Fuel, 225, 358–369. https://doi.org/10.1016/j.fuel.2018.03.167